JACC: BASIC TO TRANSLATIONAL SCIENCE VOL. 9, NO. 3, 2024

ORIGINAL RESEARCH - PRECLINICAL

Myocardial Matrix Hydrogels Mitigate Negative Remodeling and Improve Function in Right Heart Failure Model

Jervaughn D. Hunter, PhD,[a] Joshua M. Mesfin, BS,[a] Tanzeel Ahmed, BS,[a] Alexander Chen, BS,[a] Kate Reimold,[a] Arielle Hancko, BS,[a] Rebecca L. Braden, MS,[a] Michael E. Davis, PhD,[b] Karen L. Christman, PhD[a]

VISUAL ABSTRACT

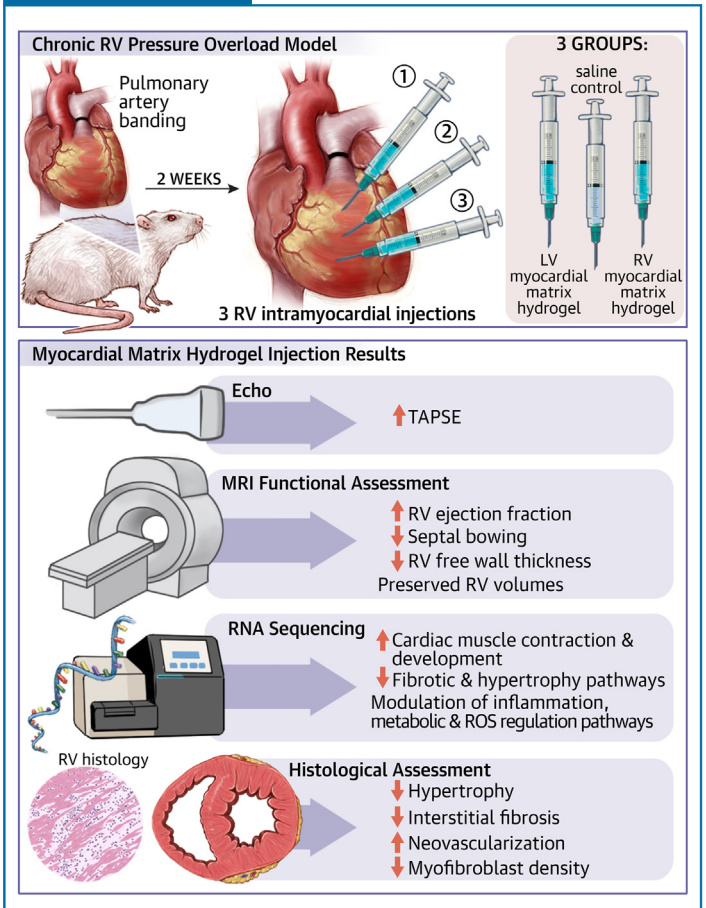

Hunter JD, et al. J Am Coll Cardiol Basic Trans Science. 2024;9(3):322-338.

HIGHLIGHTS

- **LV- and RV-derived MM hydrogels improve RV contractility over time, preserve RV volumes, and reduce RV-free wall thickness.**
- **LV-derived MM hydrogels improve RVEF.**
- **LV- and RV-derived MM hydrogels reduce hypertrophy and interstitial fibrosis, decrease myofibroblast density, and enhance neovascularization.**
- **Although both MM hydrogels enhance gene expression related to neovascularization, contractility, and cardiac development, the RV-derived MM hydrogel enhances inflammatory and fibrotic gene expression, suggesting greater therapeutic benefit of the LV-derived MM hydrogel.**

From the [a]Shu Chien-Gene Lay Department of Bioengineering and Sanford Consortium for Regenerative Medicine, University of California-San Diego, San Diego, California, USA; and the [b]Wallace H. Coulter Department of Biomedical Engineering, Georgia Institute of Technology and Emory University, Atlanta, Georgia, USA.

ISSN 2452-302X https://doi.org/10.1016/j.jacbts.2024.01.006

SUMMARY

This study evaluates the effectiveness of myocardial matrix (MM) hydrogels in mitigating negative right ventricular (RV) remodeling in a rat model of RV heart failure. The goal was to assess whether a hydrogel derived from either the right or left ventricle could promote cardiac repair. Injured rat right ventricles were injected with either RV-or left ventricular–derived MM hydrogels. Both hydrogels improved RV function and morphology and reduced negative remodeling. This study supports the potential of injectable biomaterial therapies for treating RV heart failure. (J Am Coll Cardiol Basic Trans Science 2024;9:322–338) © 2024 The Authors. Published by Elsevier on behalf of the American College of Cardiology Foundation. This is an open access article under the CC BY-NC-ND license (http://creativecommons.org/licenses/by-nc-nd/4.0/).

ABBREVIATIONS AND ACRONYMS

ECM = extracellular matrix

EDEI = end-diastolic eccentricity index

LV = left ventricular

MI = myocardial infarction

MM = myocardial matrix

MRI = magnetic resonance imaging

PAB = pulmonary artery banding

RV = right ventricular

RVEDV = right ventricular end-diastolic volume

RVEF = right ventricular ejection fraction

RVESV = right ventricular end-systolic volume

RVHF = right ventricular heart failure

SMA = smooth muscle actin

TAPSE = tricuspid annular plane systolic excursion

Congenital heart disease, ischemia, and pressure overload have all been implicated in the progression of right ventricular (RV) dysfunction in patients. Chronic pressure overload on the right ventricle ultimately leads to right ventricular heart failure (RVHF) and is most commonly a result of pulmonary arterial hypertension in the adult population and palliation to correct hypoplastic left heart syndrome in the pediatric population.[1,2]

When the right ventricle is subjected to increased afterload, it initially adapts by dilating and hypertrophying. However, ultimately, over time it begins to succumb to negative RV remodeling characterized by myocardial apoptosis, ischemia, vessel rarefaction, metabolic shifts, inflammation, fibrosis, and oxidative stress.[3-5] This negative remodeling then leads to poor contractility of the right ventricle and RVHF. Currently, treatments for RVHF are targeted at alleviating symptoms; they include medications (diuretics, angiotensin-converting enzyme inhibitors, and beta-blockers), oxygen therapy, fluid and sodium restriction, cardiac rehabilitation, surgical intervention, and palliative care.[6] Although they are effective in reducing the underlying symptoms of RVHF, none of the standards addresses the need to rescue or preserve the right ventricle and further mitigate failure. Although total heart transplantation is the only cure, the lack of donor hearts and clinically available therapeutics that mitigate RV dysfunction/failure or restore cardiac output has led to a pressing need to develop a regenerative or pro-reparative therapy to rescue the failing right ventricle.

Several researchers have investigated the use of cell therapies to treat RVHF.[7] These include neonatal c-kit cardiac-derived progenitor cells, which mitigated negative RV remodeling and improved cardiac function in small animal models of RVHF[8,9] and are currently being evaluated in the CHILD (Hypoplastic Left Heart Syndrome Study; NCT03406884) trial. Although this therapy is strategic due to the ability to isolate autologous cells and deliver them during palliative surgery, it suffers from many of the same hindrances as other cell therapies, including low survival, retention, and engraftment rates[7] as well as high expense.

We previously developed an alternative, biomaterial-based regenerative medicine therapy for heart failure that is not afflicted with the same limitations as cell therapy. Our porcine, left ventricular (LV)-derived, decellularized extracellular matrix (ECM) hydrogel, termed myocardial matrix (MM) hydrogel, has been studied extensively in small and large animal myocardial infarction (MI) models to treat negative LV remodeling.[10-14] By providing a new microenvironment that encourages endogenous cell infiltration and stimulating a pro-remodeling immune response, the MM hydrogel promotes neovascularization, mitigates fibrosis, modifies cardiac metabolism, reduces cardiac apoptosis, mitigates negative LV modeling, promotes a pro-remodeling immune response, and significantly improves cardiac function.[10,12,14-16] Furthermore, MM hydrogels have shown initial safety and feasibility in a phase 1 clinical trial in patients with subacute and chronic MI.[17] Although pressure overload is a mechanical injury, the tissue-level changes that occur in the right ventricle are similar to those of negative LV remodeling, and thus we sought to explore whether the MM material could also treat negative RV remodeling.

The authors attest they are in compliance with human studies committees and animal welfare regulations of the authors' institutions and Food and Drug Administration guidelines, including patient consent where appropriate. For more information, visit the Author Center.

Manuscript received October 25, 2023; revised manuscript received January 4, 2024, accepted January 8, 2024.

It is known that the left and right ventricles are distinct tissues based on differences in transcriptional pathways that drive their developmental origins and their differences in morphology, physiology, and molecular adaptation.[2,18] With these differences in mind, we recently developed a RV-derived MM hydrogel that was compared vs its LV counterpart and found that although the 2 materials have similar mechanical properties, they do indeed possess distinct proteomic compositions.[19] The aim of the current study was to evaluate the potential of the RV and LV MM hydrogels to mitigate negative remodeling and improve cardiac function in a small animal model of RVHF and to determine whether regional cardiac specificity of the hydrogel was important for enhancing cardiac repair. Based on the evidence of how similarly the right ventricle negatively remodels compared with the left ventricle, and because their molecular adaptations are similar, we hypothesized that our MM hydrogels would promote a pro-reparative environment within the injured right ventricle to mitigate negative RV remodeling by targeting similar pathways that we observed in the MI models. Although numerous injectable biomaterials have been evaluated for treating the failing left ventricle,[20,21] this study is the first, to the best of our knowledge, to explore the use of an injectable biomaterial for treating the failing right ventricle.

METHODS

LV AND RV MM HYDROGEL DECELLULARIZATION AND PREPARATION. MM was first obtained by isolating the left and right ventricles of hearts from 4-month-old, female, ~40 kg pigs and then processing them by following a previously published protocol.[10,19] In summary, the ventricles were washed with water, and their endocardium, epicardium, valves, papillary muscles, and large vessels were removed, resulting in homogeneous pieces of myocardium. The ventricles were then separately chopped, decellularized using a sodium dodecyl sulfate solution, lyophilized and milled into a fine powder, partially enzymatically digested using pepsin in hydrochloric acid, balanced to a neutral pH, lyophilized, and stored at -80°C.[19] When preparing for injection, lyophilized aliquots were kept on ice and reconstituted with sterile saline to a concentration of 6 mg/mL. For quality control, our LV and RV MM hydrogels were characterized as previously reported.

SURGICAL PROCEDURES. All procedures in this study were approved by the committee and performed according to the guidelines established by the Committee on Animal Research at the University of California-San Diego, and the Association for the Assessment and Accreditation of Laboratory Animal Care. To induce pressure overload in the right ventricle, a previously established pulmonary artery banding (PAB) model with 6-week-old, juvenile, male Sprague Dawley rats (180-200 g) was used.[8,9,22,23] Rats were anesthetized by using isoflurane in oxygen at 5%, intubated, and maintained at 2.5% isoflurane in oxygen during surgery. A left thoracotomy was performed, and the pulmonary artery was then isolated and partially ligated using an 8-0 silk suture and 18-gauge needle sheath as a spacer to guide the degree of stenosis. The needle was then retracted to allow antegrade flow through the band.

Two weeks after banding, animals were arbitrarily assigned to treatment groups that received 3 25-μL injections of either saline, LV MM, or RV MM. Rats were anesthetized as mentioned earlier and placed in a supine position where an incision was made from the xyphoid process along the abdomen and an incision was then made in the diaphragm to expose the apex of the heart, leaving the sternum intact.[10,11] Three intramyocardial injections were then delivered evenly throughout the RV free wall from apex to base.

Two cohorts of animals were used for the following studies: Cohort 1, echocardiography, cardiac magnetic resonance imaging, and long-term histology (~4.5 weeks' postinjection); and Cohort 2, RNA-sequencing and short-term histology (1 week postinjection).

ECHOCARDIOGRAPHY. Echocardiography was used to evaluate heart function of rats with PAB during banding, at injection, and at 2 and 4 weeks' postinjection. Healthy animals (nonbanded) were also imaged alongside the banded animals at the aforementioned time points. Animals were maintained at 2.5% isoflurane in oxygen during the duration of imaging. A Vivid I portable digital high-frequency ultrasound system (GE Healthcare) equipped with an i12L-RS transducer probe (GE Healthcare) was used to perform transthoracic echocardiography. Tricuspid annular plane systolic excursion (TAPSE) of the lateral region was acquired in apical 4-chamber view by M-mode.[9]

CARDIAC MAGNETIC RESONANCE IMAGING. Cine cardiac magnetic resonance images were obtained via the Molecular Imaging Center at Sanford's 11.7 T Horizontal Bruker BioSpec Magnetic Resonance Imaging System (Bruker). Acquired images were used to evaluate cardiac morphology, volumes, and function of the animals. Rats were anesthetized by using

isoflurane in oxygen during imaging. Respiratory and electrocardiogram-gated cine sequences were acquired over contiguous heart axial slices. The following parameters were used: repetition time = 10 milliseconds; echo time = 2 milliseconds; flip angle = 30°; field of view = 50 mm^2; and data matrix size = 250 × 250. Seven 1.5-mm axial image slices were acquired with a total of 10 cine frames per image slice. Minimum and maximum RV lumen area were determined by using Fiji (Fiji is Just ImageJ, National Institutes of Health [NIH]) software to trace the endocardial surface at end-diastole and end-systole for each slice, respectively.

Simpson's method was used to determine RV end-diastolic volume (RVEDV) and RV end-systolic volume (RVESV).[24] RV ejection fraction (RVEF) was calculated as: ([RVEDV - RVESV]/RVEDV) × 100. The RV myocardium was defined as the area between the RV free wall's endocardium and epicardium excluding the papillary muscles, trabeculations, and trabecula septomarginalis. Morphology of the pressure overloaded right ventricle can be characterized by assessing the curvature of the interventricular septum. Short-axis, cardiac magnetic resonance images at the mid ventricular region at end-diastole and end-systole were used to determine the LV end-diastolic eccentricity index (EDEI) and LV end-systolic eccentricity index as previously described.[25] To quantify the eccentricity index, 2 diameters were measured: one tracing the diameter from the mid septal wall to the LV free wall (D1) and the other trace connecting the LV endocardial surfaces intersecting D1 perpendicularly (D2) while ignoring papillary muscles. The intersection of D1 and D2 were ensured to be perpendicular at the center of the LV lumen. The ratio of D2/D1 in healthy animals is 1, and thus any measurement >1 indicates a flattened interventricular septum.

To evaluate RV free wall thickness, short-axis cine images were taken at end-diastole, and the length of lines drawn at the thickest region of the inferior and anterior free wall was averaged.[26] The sum of those averages was then reported as the total RV free wall thickness.[26]

TISSUE PROCESSING. At 31.5 ± 3.5 days (~4.5 weeks') postinjection, animals used for functional analysis were euthanized via intraperitoneal injection of Fatal-Plus (Vortech Pharmaceuticals) at 1 mL of solution per 4.5 kg of body weight of the animal, and their hearts were excised and frozen in Tissue-Tek O.C.T. Compound (Sakura Finetek). Frozen, embedded hearts were then cryosectioned into 10-μm thick sections. A second set of animals (n = 5-6 per group) were euthanized via intraperitoneal injection of Fatal-Plus at 1 mL of solution per 4.5 kg of body weight of the animal at 1 week postinjection, and their hearts were sliced into 6 1-mm thick slices using a stainless-steel rat heart slicer matrix (Zivic Instruments) with 1.0-mm coronal spacing. The right ventricle was isolated from the even slices and flash frozen in liquid nitrogen to preserve RNA.[14] All odd slices were frozen in Tissue-Tek O.C.T. and stored at -80°C.

BULK RNA-SEQUENCING. Messenger RNA from RV tissue flash frozen in liquid nitrogen was isolated by using the RNeasy Fibrous Tissue Mini Kit and the QIAcube Connect nucleic acid isolation robot (Qiagen) 1 week postinjection. Purified messenger RNA was pooled by combining 2 biological replicates into 1 such that n = 3 per treatment group; this was analyzed by using a TapeStation 2200 with a high-sensitivity RNA ScreenTape (Agilent). After the RNA integrity number was confirmed to be adequate, the RNA was processed using the Illumina Stranded mRNA Prep kit. Libraries were quantified via a Qubit 3.0 (Thermo Fisher Scientific), and fragment size was determined by using a TapeStation 2200 with a D5000 ScreenTape. Libraries were then sequenced on a NextSeq 2000 system (Illumina) at a depth of 75 × 2. Differential expression analysis was conducted by using the onboard Dragen RNA version 3.10.12 pipeline (Illumina) comparing all detected aligned genes from the *Rattus norvegicus* genome.

MACROPHAGE DENSITY ANALYSIS. Slides from animals survived 1 week postinjection were used to quantify macrophage density. Two locations from the apex, mid ventricular region, and base were taken, and 2 slides were taken at each location with a total of 4 to 6 tissue sections for each stain. Immunohistochemistry was performed by using antibodies for CD68 (1:300; Abcam) and CD163 (1:300; Bio-Rad) incubated with goat anti-rabbit immunoglobulin G conjugated Alexa Fluor 750 (1:500; Invitrogen) and goat anti-mouse immunoglobulin G conjugated Alexa Fluor 594 (1:500; Invitrogen), respectively. Slides were then mounted using Fluoromount (Sigma-Aldrich) and scanned at 20× magnification using an VS200 fluorescent slide scanner (Olympus Life Science). Macrophages were quantified as total number of $CD68^+$ cells colocalized with 4′,6-diamidino-2-phenylindole, total number of $CD163^+$ cells co-localized with 4′,6-diamidino-2-phenylindole, and ratio of total number of CD163/CD68 using cell counter analysis in the QuPath version 0.4.3 software.

HYPERTROPHY ANALYSIS. Hearts harvested at ~4.5 weeks' postinjection were sectioned starting at

the apex, with 18 locations taken and 6 slides per location to span the entire right ventricle. Slides were stained with tetramethylrhodamine-labeled wheat germ agglutinin (1:20; Vector Laboratories) to identify cardiomyocyte boundaries, and Hoechst 33342 (1:1000; Life Technologies) was used to identify nuclei. Slides were then mounted using Fluoromount and scanned at 20× magnification using an VS200 fluorescent slide scanner. Cross-sectional area of cardiomyocytes in the mid wall of the right ventricle was assessed along their major axes and measured by using Fiji.

FIBROSIS ANALYSIS. Slides were stained with Masson's trichrome, mounted with Permount Mounting Medium (Fisher Chemical), and scanned at 20× magnification using an Olympus VS200 brightfield slide scanner (Evident Scientific). Six representative evenly spaced slices throughout the mid ventricular region of the right ventricle were used to assess free wall fibrosis. Nonnuclear blue stain was identified as the fibrotic region of the tissue slices and was quantified by using color deconvolution and pixel classifier via the QuPath software. Percent fibrosis was calculated as fibrotic area in the right ventricle/total area of the right ventricle.

ARTERIOLE AND MYOFIBROBLAST DENSITY. Fluorescein labeled Griffonia Simplicifolia Lectin I isolectin B4 (1:75; Vector Laboratories) was used to identify endothelial cells within the right ventricle, α-smooth muscle actin (α-SMA) (1:75; Dako) was used to identify smooth cells, and Hoechst 33342 (1:1000; Life Technologies) was used to identify nuclei. Slides were then mounted by using Fluoromount and scanned at 20× magnification using an Olympus VS200 fluorescent slide scanner. Arteriole and myofibroblast density was quantified by manually counting in 5 evenly distributed regions throughout the right ventricle in 6 slides (evenly spaced throughout the RV mid ventricular region) using Fiji. Arterioles were identified based on the following criteria: 1) co-staining of isolectin and α-SMA; 2) presence of a visible lumen; and 3) Feret diameter >10 μm as previously described.[10,14] Capillaries were identified as percent positive area of isolectin not co-localized with α-SMA. Myofibroblasts were identified as cells staining positive for α-SMA and not found in vessels.[15]

STATISTICAL ANALYSIS. Data are reported as mean ± SEM. Two-way repeated measures analysis of variance was used to compare within- and between-treatment group echocardiographic changes over time, using Tukey's post hoc test for multiple pairwise comparisons. To compare treatment groups from magnetic resonance imaging (MRI), histology, and immunohistochemistry, a 1-way analysis of variance with Tukey's post hoc test was used. Pearson correlation coefficients (r) were used to quantify the association between continuous data in both imaging modalities. Using R's DESeq2 library, differentially expressed genes were identified as average log(fold-change) >0.6 and adjusted P value <0.10 for up-regulated genes, and average log(foldchange)>-0.6 and adjusted P value <0.10 for down-regulated genes. Adjusted P values were determined via Benjamini-Hochberg's method. Statistical significance was accepted at a P value <0.05.

RESULTS

LV MM AND RV MM HYDROGELS IMPROVE RV SYSTOLIC FUNCTION AS EVIDENCED BY ECHOCARDIOGRAPHY. We first evaluated the effects of our MM hydrogels on RV function in a small animal model of RVHF using clinically relevant imaging modalities.[27,28] RV function was evaluated longitudinally via echocardiography in animals that underwent PAB and their nonbanded counterparts. All animals exhibited equal TAPSE (measure of RV systolic function) before the banding time point (Figure 1). At 2 weeks' postbanding, all banded animals displayed a significantly reduced TAPSE compared with their nonbanded counterparts, indicating a successful induction of injury. Reparative effects were first observed as early as 2 weeks' postinjection when comparing both LV MM-treated animals and RV MM-treated animals vs the saline control. It was observed that animals injected with either LV MM or RV MM showed significant improvements in TAPSE at 2 and 4 weeks' postinjection.

LV MM AND RV MM HYDROGELS MITIGATE NEGATIVE RV REMODELING AND IMPROVE RV FUNCTION AS EVIDENCED BY MRI. Morphology and overall function are known to be affected during pressure overload of the ventricle.[29,30] Because of this, we used MRI to further elucidate and confirm the effects of our MM hydrogels on the failing right ventricle. Endpoint MRI was performed ∼4.5 weeks after injection of saline (n = 8), LV MM (n = 8), or RV MM (n = 9). Representative short-axis cine images of saline-, LV MM-, and RV MM-treated animals at end-diastole and end-systole are presented in Figure 2A. Both LV MM- and RV MM-treated animals showed significant decreases in RVEDV (Figure 2B) and RVESV (Figure 2C) compared with animals treated with saline. In addition, when assessing the pumping capacity of the right ventricle, animals treated with the LV MM hydrogel showed a significant increase in RVEF

FIGURE 1 LV MM and RV MM Hydrogels Improve Systolic Function Over Time

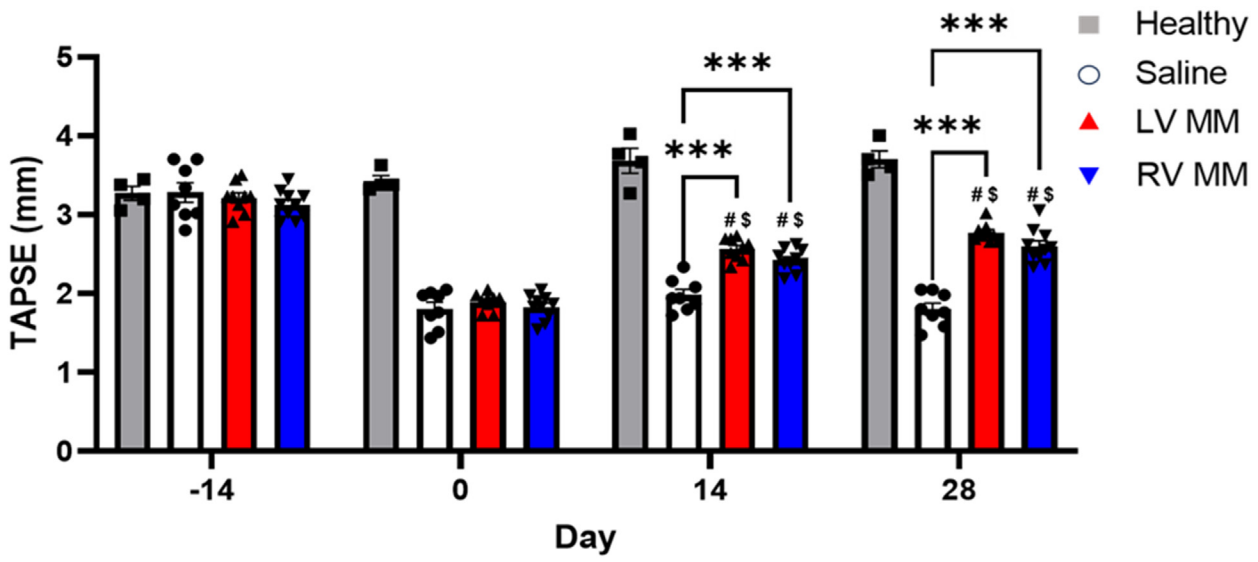

Echocardiographic imaging shows that both myocardial matrix (MM) hydrogels improve tricuspid annular plane systolic excursion (TAPSE) over saline control and over time. At the time of banding (day -14), all animal groups exhibited healthy TAPSE. At the time of injection (day 0), all banded animals had significantly reduced TAPSE. At day 14 and day 28, animals treated with either the left ventricular (LV)-derived MM hydrogels or the right ventricular (RV)-derived MM hydrogel showed significantly improved TAPSE compared with the saline control at the respective time point. Data are presented as mean ± SEM. N = 9-10. ***$P < 0.001$ compared with saline-treated animals at the respective time point, #$P < 0.05$ compared with saline-treated animals at the injection time point, and \$$P < 0.05$ compared with the same treatment at the prior time point with 2-way repeated measures analysis of variance with Tukey's post hoc test.

(Figure 2D) compared with those injected with saline. Although not significant, trending improvements in RVEF were noted in animals treated with the RV MM hydrogel. When assessing morphology, animals treated with the LV MM hydrogel had significantly lower LV EDEIs than those treated with saline, whereas animals treated with the RV MM hydrogel had trending (Figure 2E) lower LV EDEIs vs saline. There were no significant differences in LV end-systolic eccentricity index (Figure 2F). In addition, both the LV MM- and RV MM-treated groups had significantly thinner RV free walls than their saline-treated counterparts (Figure 2G).

FUNCTIONAL IMPROVEMENTS CORRELATE BETWEEN IMAGING MODALITIES. Echocardiography and MRI are the main modalities used to assess RV function in the clinic. Alone, these tools give insight into cardiac health; confirming trends between the two is a robust means for making claims of therapeutic benefit. Thus, we plotted the echocardiographic data (x-axis) against MRI readings (y-axis) to show trends per condition. We found r values of -0.71 and -0.87 for RVEDV and RVESV with TAPSE, respectively, indicating a negative correlation between TAPSE and volumes. We further observed clear clustering of LV MM and RV MM treatment groups, with saline control animals exhibiting larger volumes and reduced TAPSE (Figures 3A and 3B). In addition, TAPSE and RVEF were positively correlated, as evidenced by an r value of 0.85 (Figure 3C). Similar clustering of both MM treatment groups was noted, with improved RVEF and TAPSE while saline clustered inversely. Finally, wall thickness was also negatively correlated with TAPSE, as evidenced by r = -0.91, and LV MM and RV MM clustered again with reduced RV free wall thickness being related to improved TAPSE (Figure 3D).

GENE EXPRESSION ANALYSIS REVEALS LV MM AND RV MM HYDROGELS MODULATE PATHWAYS RELEVANT TO CARDIAC REPAIR. The failing right ventricle has been described as having inadequate microvasculature, increased ischemia and inflammation, oxidant/anti-oxidant imbalance, adaptive and maladaptive hypertrophy, modified cardiac metabolism, impaired cardiac growth, autophagy, apoptosis. and fibrosis.[3,30] We therefore used bulk RNA-sequencing to evaluate differential gene expression analysis in RV tissue from animals treated with saline (n = 5), LV MM (n = 6), and RV MM (n = 6) 1-week post-injection. Each biological replicate was pooled such that n = 3 per group based on evidence that there is no loss in differential gene expression when pooling

FIGURE 2 LV MM and RV MM Hydrogels Mitigate Negative RV Remodeling and Improve RV Function

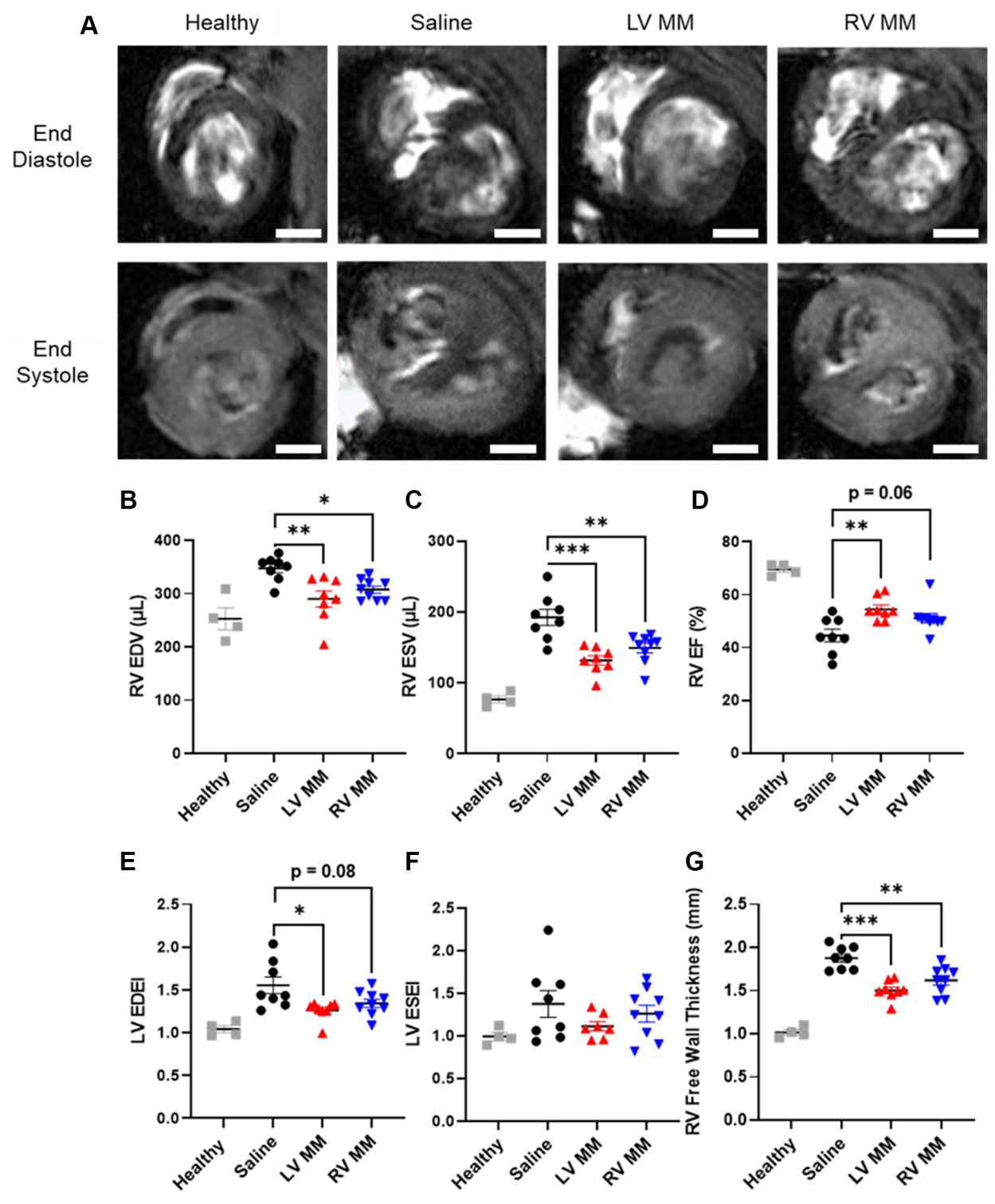

(A) Short axis: representative images of study animals show the right ventricle (upper left of each image) of each treatment group at end-diastole. RV volumes, ejection fraction, and morphology were quantified by assessing changes in RV end-diastolic volume (RVEDV) (B), RV end-systolic volume (RVESV) (C), RV ejection fraction (RVEF) (D), LV end-diastolic eccentricity index (LVEDEI) (E), LV end-systolic eccentricity index (LVESEI) (F), and RV free wall thickness (G). Scale bar = 2 mm. Data are presented as mean ± SEM. N = 8-9. *$P < 0.05$, **$P < 0.01$, and ***$P < 0.001$ compared with saline-treated animals with 1-way analysis of variance with Tukey's post hoc test. Abbreviations as in Figure 1.

FIGURE 3 **Functional Improvements Correlate Between Imaging Modalities**

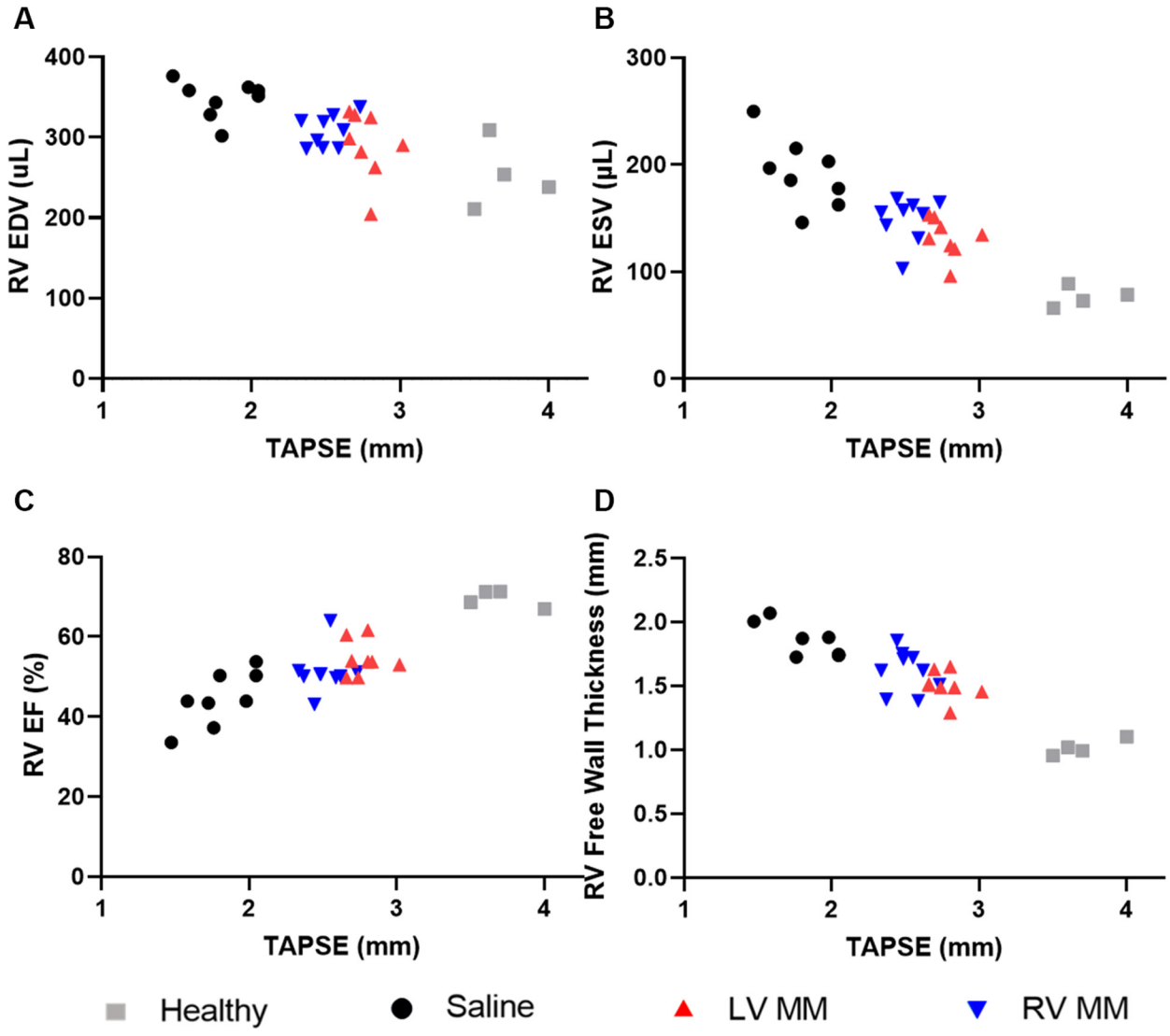

Data from echocardiography and magnetic resonance imaging were compared to show the conserved functional benefit of each hydrogel. (A and B) Animals treated with LV MM or RV MM hydrogels showed clear separation from saline control group by exhibiting increased TAPSEs and reduced RVEDV ($r = -0.71$; $P \leq 0.001$) (A) and RVESV ($r = -0.87$, $P \leq 0.001$) (B). (C) Animals treated with the LV MM or RV MM hydrogel also showed clustering improvements in the 2 main measures of RV function (RVEF and TAPSE) ($r = 0.85$; $P \leq 0.001$) being clearly separated from the saline-treated group. (D) Correlation plot reveals that animal treated with LV MM or RV MM hydrogels clustered with thinner right ventricles and higher TAPSEs than saline-treated animals ($r = -0.91$; $P \leq 0.001$). N = 8 to 9. Abbreviations as in Figures 1 and 2.

the RNA of biological replicates.[31,32] At 1 week postinjection, there is peak cell infiltration in the MM hydrogel[12]; in previous studies in rat subacute[14] and chronic[15] MI models, substantial differences were found in gene expression in animals treated with the LV MM hydrogel at this time point. Enhanced volcano plots showing the differential gene expression of animals treated with the LV MM hydrogel compared with those treated with saline (98 differentially expressed) and the RV MM hydrogel vs the saline control (275 differentially expressed) are presented in Figures 4A and 4B, respectively. Based on gene ontology enrichment analysis, we found that both the LV MM (Figure 4C) and the RV MM (Figure 4D) hydrogel affect pathways relevant to cardiac repair, including circulatory system development, muscle structure development, defense response, regulation of immune response, vasculature development, and cellular response to oxygen containing compound.

FIGURE 4 Differential Gene Expression at 1 Week Postinjection

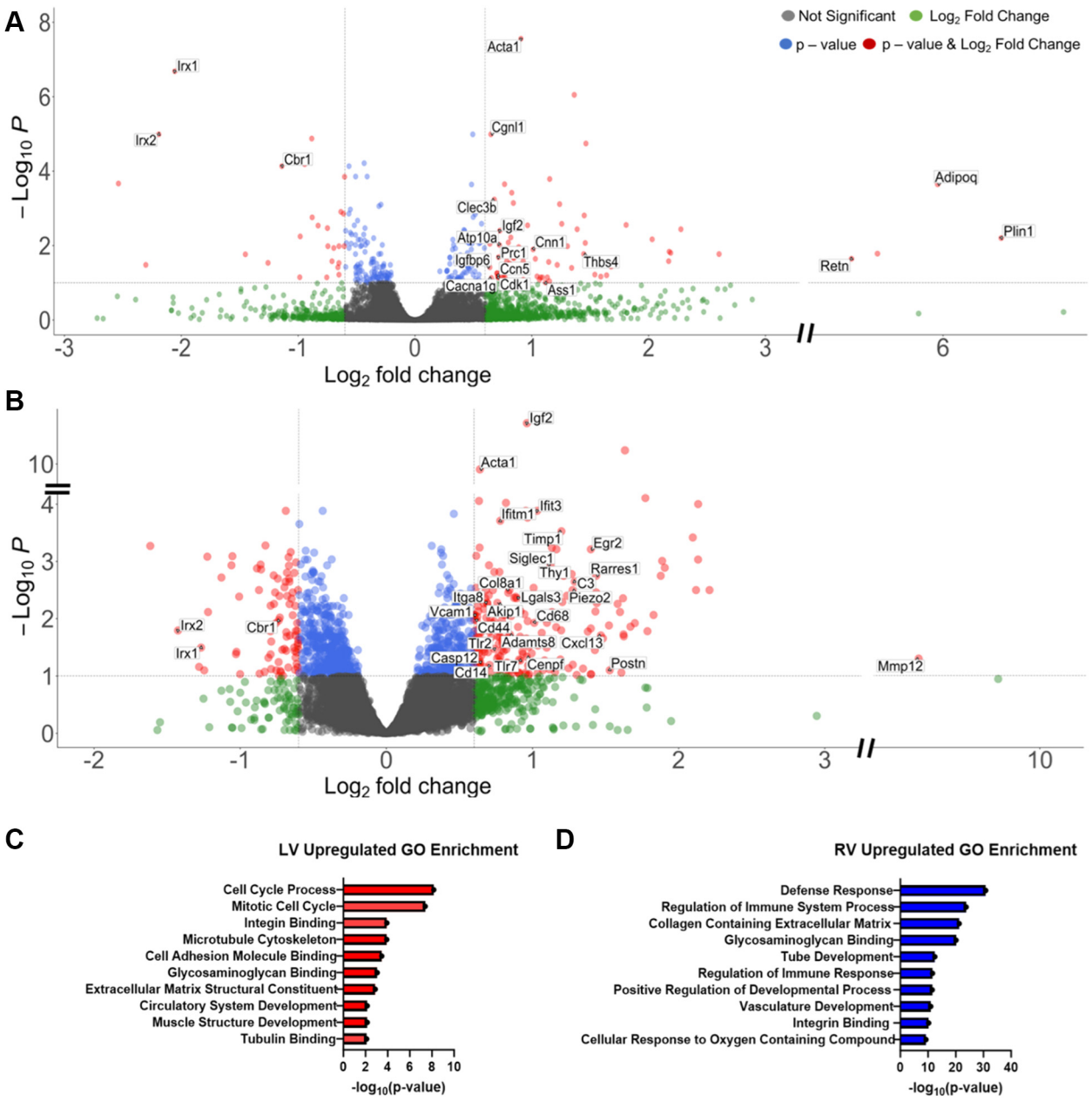

(A) Enhanced volcano plot reveals 98 differentially expressed genes comparing LV MM and saline-treated animals. (B) Enhanced volcano plot shows that animals treated with the RV MM hydrogel exhibited 275 differentially expressed genes compared with saline. Gene ontology (GO) analysis reveals pathways affected by LV MM (C) and RV MM (D) treatments compared with saline-treated animals. N = 5-6. Abbreviations as in Figure 1.

Previously published studies with the LV MM hydrogel as well as decellularized ECM biomaterials in general show that these biomaterials are pro-reparative and anti-inflammatory[14,20,33,34]; similarly, we found that the LV MM hydrogel promoted a pro-remodeling/anti-inflammatory immune phenotype with the overexpression of Slfn4, Igf2, and Igfbp6. Interestingly, although the RV MM hydrogel also increased expression of anti-inflammatory genes (Igf2 and Sln4), it additionally led to up-regulation of many pro-inflammatory genes (Aif1, Casp12, Cxcl13, CD14, CD44, CD68, C2, C3, Egr1, Egr2, Ifitm1, Ifit3, Tlr2, Tlr7,

and S100a9). Both materials up-regulated genes that were related to neovascularization (LV MM hydrogel: Acta1, Cgnl1, and Cnn1; RV MM hydrogel: Acta1, Apold1, and Vcam1). Although the LV MM-treated groups overexpressed antifibrotic genes (Clec3b, Cdk1 and Ccn5), the RV MM hydrogel up-regulated the pro-fibrotic genes (Adamts8, Col11a1, Col18a1, Col7a1, Col8a1, Col8a2, Mmp12, Timp1, Lox, Lox1, and Postn) compared with the saline-treated animals. Furthermore, in terms of cardiac development and contractility, the LV MM hydrogel induced the overexpression of Atp10a, Cacna1g, Chodl, and Prc1, whereas RV MM-treated animals overexpressed Akip1, Piezo2.

Supplemental Table 1 lists all the differentially expressed genes between LV MM and saline; Supplemental Table 2 lists the genes regulated between RV MM and saline. There were no relevant differentially expressed genes comparing LV MM-treated animals vs RV MM-treated animals (Supplemental Table 3).

LV MM AND RV MM HYDROGELS AFFECT ARTERIOLE DENSITY BUT NOT MACROPHAGE, CAPILLARY, OR MYOFIBROBLAST DENSITY AT 1 WEEK POSTINJECTION. It has been shown that bone marrow–derived monocytes are recruited into the right ventricle during pressure overload,[35] and $CD68^+$ macrophages have been linked with dilation and cardiac dysfunction in models of RV pressure overload.[36] Here, we evaluated whether our materials could modulate the number of macrophages within the right ventricle 1 week after injection and if macrophages were encouraged to polarize into the M2-like phenotype ($CD163^+$). **Figure 5A** shows a representative image of CD68 and CD163 macrophages in the right ventricle. In **Figures 5B to 5D**, we saw no significant differences in $CD68^+$ or $CD163^+$ macrophages, and although there were more CD163 macrophages in number, there was no significant difference in the ratio of these 2 phenotypes between the groups.

Vessel formation and myofibroblast activation were also evaluated 1 week after injection (**Figures 5E to 5G**). Although animals treated with LV MM or RV MM had significantly greater arteriole density (**Figure 5H**) than saline-treated animals, there was no significant difference in capillary density (**Figure 5I**) or myofibroblast density (**Figure 5J**).

LV MM AND RV MM HYDROGELS REDUCE CARDIOMYOCYTE HYPERTROPHY, MITIGATE INTERSTITIAL FIBROSIS, REDUCE MYOFIBROBLAST DENSITY, AND IMPROVE ARTERIOLE DENSITY AT 4.5 WEEKS' POSTINJECTION. During the negative remodeling of the pressure overloaded right ventricle, there is a key shift from adaptive hypertrophy to maladaptive hypertrophy.[3,27] While initially compensatory, when exposed to chronic stressors such as sustained increase in afterload, this maladaptive hypertrophy leads to an excessive increase in the dimensions of the right ventricle, which leads to fibrosis and myocardial dysfunction.[37] Representative images of the cardiomyocyte cross-sectional area are shown in **Figures 6A to 6D**. As seen in **Figure 6E**, there was a significant decrease in the cardiomyocyte cross-sectional area in animals treated with the LV MM or RV MM hydrogel compared with animals treated with saline.

It has been shown that MM hydrogels can mitigate fibrosis in models of subacute[12] and chronic[15] MI. Because it has also been shown that a similar cascade of fibrosis develops when the right ventricle fails,[30,38] we sought to determine if our LV MM or RV MM hydrogels would mitigate fibrosis in an RVHF model. Representative images of interstitial fibrosis within the mid ventricular region of the RV free wall of saline-, LV MM-, and RV MM-treated animals are presented in **Figures 6F to 6I**, respectively. LV MM- and RV MM-treated animals had a significant reduction in RV free wall fibrosis compared with the saline control (**Figure 6J**).

Vasculature rarefaction[27] and myofibroblast activation and infiltration[38] have been identified as major contributors to the progression of negative RV remodeling in cases of the pressure overloaded right ventricle. The current study sought to identify if animals treated with the MM hydrogels could increase vascular density while also reducing the presence of myofibroblasts. Representative images of arteriole and myofibroblast density within the mid ventricular region of the RV free wall of saline-, LV MM-, and RV MM-treated animals are presented in **Figures 7A to 7D**, respectively. Animals treated with LV MM or RV MM hydrogels displayed a significantly greater number of arterioles throughout the RV free wall compared with animals treated with saline as shown in **Figure 7E**. There was no difference in capillary density seen between the groups (**Figure 7F**). In terms of myofibroblasts, saline-treated animals had significantly greater myofibroblast density compared with either MM material (**Figure 7G**).

DISCUSSION

Although cell therapies have been evaluated in pediatric models of RVHF,[8,9] biomaterial-based reparative strategies have not been previously explored in RVHF models overall. Alternatively, porcine ECM hydrogels have been thoroughly investigated in small and large animal models and in the

FIGURE 5 LV MM and RV MM Hydrogels Affect Vascularization and Not Myofibroblast and Macrophage Density at 1 Week Postinjection

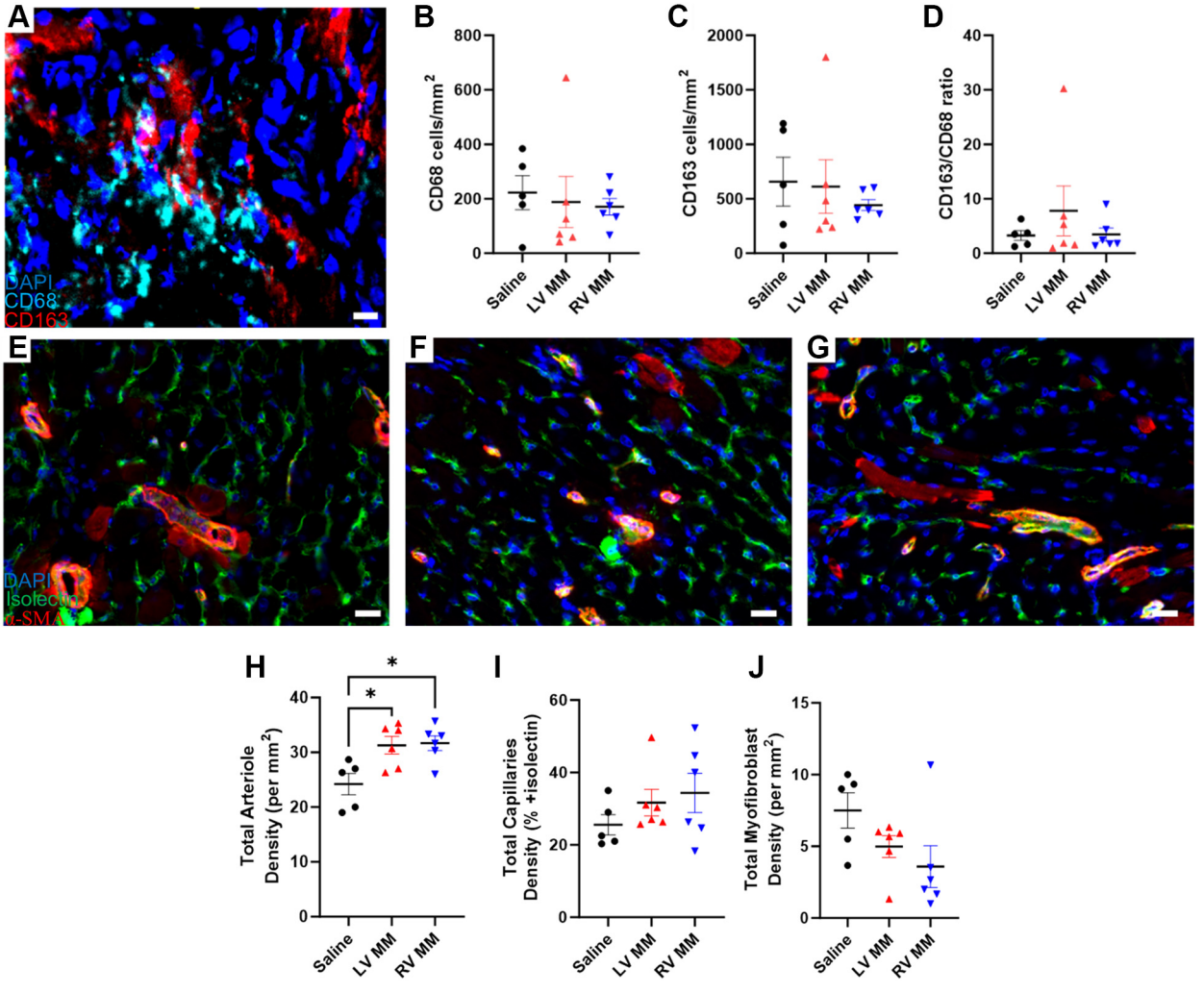

(A) Representative image of CD68$^+$ (cyan) and CD163$^+$ (red) macrophages in the right ventricle. Scale bar = 20 μm. There were no differences in CD68 density (B), CD163 density (C), or CD163/CD68 ratio (D) between the groups. Representative images of endothelial cell staining (green; isolectin), smooth muscle cells (red; α-smooth muscle actin [SMA]), and nuclei (blue; 4′,6-diamidino-2-phenylindole [DAPI]) of saline-treated (E), LV MM–treated (F), and RV MM–treated (G) hearts. (H) LV MM– and RV MM–treated animals showed greater arteriole growth than saline-treated animals. There was no difference in capillary density (I) or myofibroblast density (J) between the groups. Scale bar = 50 μm. Data are presented as mean ± SEM. *$P < 0.05$ compared with saline-treated animals with 1-way analysis of variance with Tukey's post hoc test. Abbreviations as in Figure 1.

clinic.[10-12,14,20,34,39,40] Because the LV MM hydrogel had been shown to successfully reduce negative LV remodeling and improve LV function,[12,14,15] the goal of the current study was to evaluate whether the pro-reparative properties of the material would also reduce negative RV remodeling in a model of RVHF and to further explore whether sourcing the material from the right ventricle vs the left ventricle affected cardiac repair.

To first confirm efficacy of our MM hydrogels in the rat PAB model of RVHF, echocardiography was used to evaluate wall motion and overall systolic function. The first evidence of repair was noted as early as 2 weeks' postinjection in animals treated with the LV MM or RV MM hydrogel compared with their saline counterparts with further increases in TAPSE at 4 weeks' postinjection; this is a time point after complete material degradation[12] and suggests sustained cardiac repair over time. To further confirm these functional improvements, MRI was used to assess morphology, volumes, and function at the terminal time point (~4.5 weeks' postinjection). Both

FIGURE 6 **LV MM and RV MM Hydrogels Reduce Hypertrophy and Interstitial Fibrosis in the RV Free Wall at 4.5 Weeks' Postinjection**

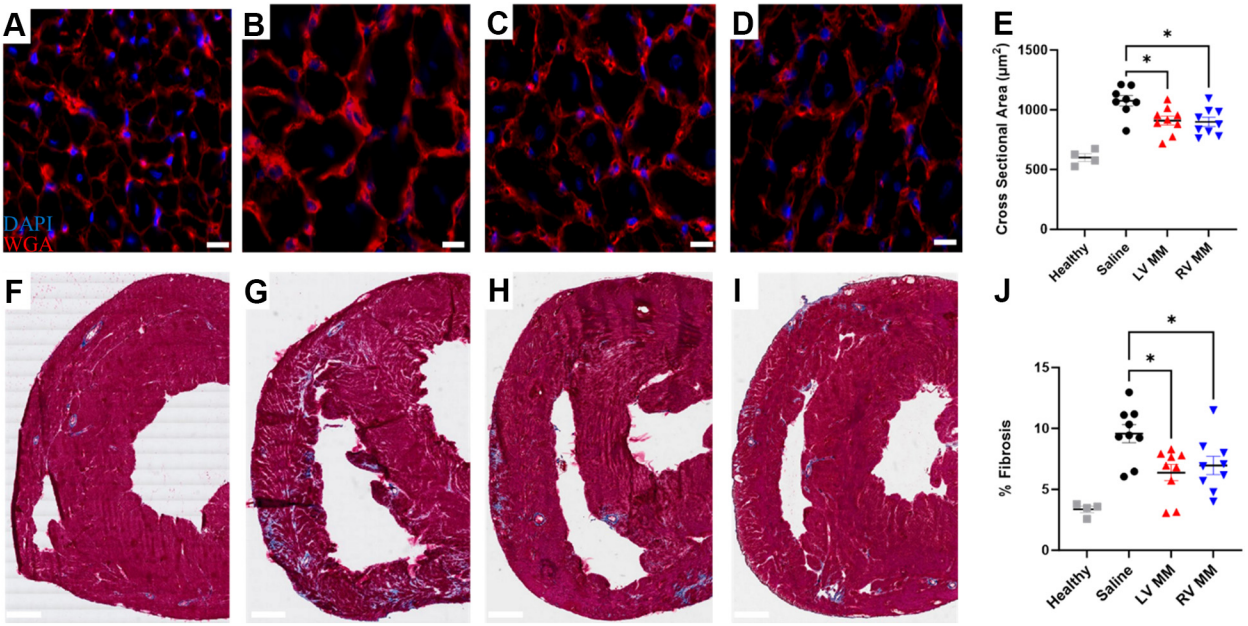

Representative images of cardiomyocyte cell boundary staining (red; wheat germ agglutinin) and nuclei (blue; DAPI) of healthy (A), saline-treated (B), LV MM–treated (C), and RV MM–treated (D) hearts. (E) Animals with either MM hydrogel exhibited significantly smaller cardiomyocyte cross-sectional areas than animals treated with saline. Scale bar = 50 μm. Representative images of Masson's trichrome staining of healthy (F), saline-treated (G), LV MM–treated (H), and RV MM–treated (I) hearts. (J) Animals treated with either MM hydrogel displayed significantly less RV free wall fibrosis. Scale bar = 2 mm. Data are presented as mean ± SEM. *$P < 0.05$ compared with saline-treated animals with 1-way analysis of variance with Tukey's post hoc test. Abbreviations as in Figures 1 and 5.

the LV MM and the RV MM hydrogel were able to reduce volumes at the terminal time point compared with animals treated with saline. A significant increase in RVEF was also observed in animals treated with the LV MM hydrogel vs saline.

In the pressure-overloaded right ventricle, morphologic maladaptation such as increased RV wall thickness and septal wall flattening occur that severely limit cardiac output.[2,3,29,30] In the current study, animals that were treated with the LV MM hydrogel had reduced LV EDEI compared with those treated with saline, suggesting a morphologic rescue. Animals treated with the RV MM hydrogel showed trending improvements in LV EDEI compared with saline; these improves were not significant, however, and were not statistically different from LV MM-treated animals. Ultimately, it was also revealed that animals treated with either of our MM hydrogels exhibited significantly thinner RV free walls than those of the saline control, further confirming rescue from morphologic maladaptation. Finally, to ensure that trends in cardiac repair were robust, we showed that improvements in echocardiographic outputs correlated with the MRI data, which also suggested that the LV MM hydrogel had slightly better outcomes than the RV MM hydrogel.

We next evaluated whether both MM hydrogels affected similar pathways and cell types relevant to cardiac repair that we had previously observed with the LV MM hydrogel in MI models. Using RNA-sequencing, differential gene expression was found in both MM hydrogel-treated groups compared with saline, including many genes relevant to cardiac repair, whereas there were limited differences between the 2 materials.

When they are appropriately decellularized, porcine ECM biomaterials are known to promote a pro-remodeling immune response characterized by M2 macrophages and T helper 2 cells and have a good safety record in patients.[33,34,39] Similarly, our LV MM hydrogel has been thoroughly investigated in small and large animal models, including in a humanized mouse model[10-12,14-16] showing a pro-remodeling immune response as opposed to pro-inflammatory immune response. Although no changes were observed in the number of macrophages at 1 week postinjection

FIGURE 7 LV MM and RV MM Hydrogels Increase Arteriole Density and Reduce Myofibroblast Density in the RV Free Wall at 4.5 Weeks' Postinjection

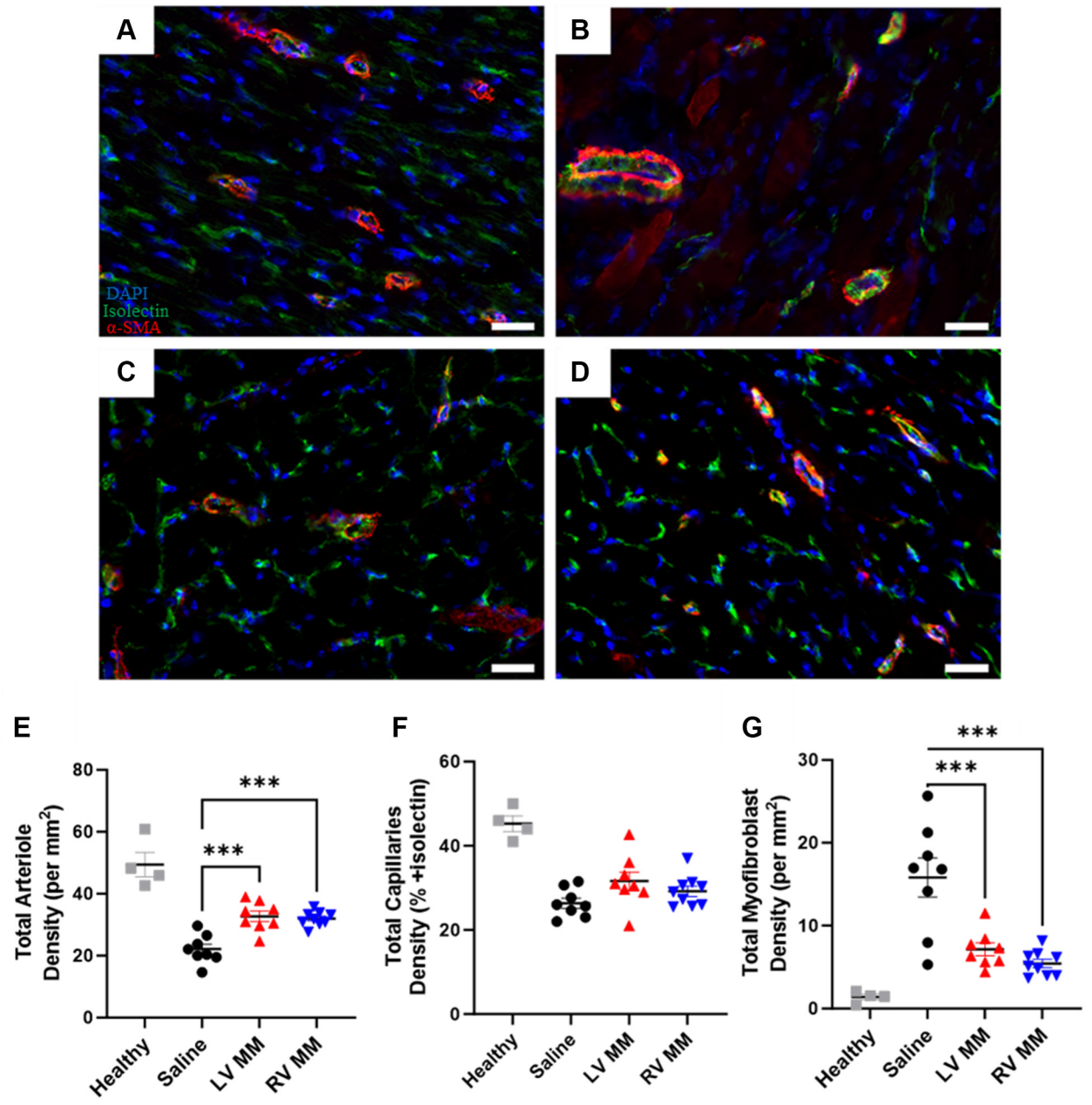

Representative images of endothelial staining (green; isolectin), smooth muscle cells (red; α-SMA), and nuclei (blue; DAPI) of healthy (A), saline-treated (B), LV MM–treated (C), and RV MM–treated (D) hearts. (E) Animal treated with either the LV MM or the RV MM hydrogel exhibited greater arteriole growth compared with saline. (F) There was no difference in capillary density between the groups. (G) LV MM- and RV MM-treated animals had significantly less myofibroblast density than saline-treated animals. Scale bar = 50 μm. Data are presented as mean ± SEM. ***$P < 0.001$, compared with saline- treated animals with 1-way analysis of variance with Tukey's post hoc test. Abbreviations as in Figures 1 and 5.

in the current study, differences were noted in genes related to inflammation. Animals treated with the LV MM hydrogel overexpressed C6, which is present on resident macrophages involved in damage-associated patterns, inflammatory cytokines, and phagocytosis[41]; however, it mainly overexpressed protective and anti-inflammatory genes such as Slfn4, Igf2, and Igfbp6.[42-44] Animals treated with the RV MM

hydrogel overexpressed Ccl2 and Ccl7, which recruit monocytes and mediate inflammatory response, respectively.[45,46] It was also noted that RV MM-treated animals overexpressed Cxcl3, which has been shown to be expressed on pro-reparative B cells.[47] The RV MM hydrogel, however, also overexpressed genes that have been linked to inflammatory cell types and innate inflammation such as CD68, Aif1, CD14, CD44, Egr2, Ifitm1, Ifit3, Tlr2, and Tlr7.[48-54] This suggests that the LV MM hydrogel is pro-reparative and anti-inflammatory, whereas the RV MM hydrogel is more pro-inflammatory, at least at 1 week postinjection. Given the still positive effects on negative RV remodeling and cardiac function, it is possible that a shift to a pro-remodeling immune response may occur later with the RV material.

Due to the vascular rarefaction that occurs in the pressure overloaded right ventricle,[27] one potential therapeutic target is increasing vascularization. Injectable hydrogels, especially ECM derived, have been shown to promote neovascularization.[14,55,56] Gene expression analysis revealed that LV MM-treated animals overexpress Cgnl1, which is enriched in endothelial cells during vascular growth,[57] and Cnn1, which is responsible for vascular smooth muscle growth.[58] RV MM-treated animals overexpress CD44, which has been known to induce vascularization during MI,[59] and also overexpressed Vcam1, which promotes angiogenesis in conjunction with Tnfα.[60] Immunohistochemistry further revealed increases in arterioles within the right ventricle with MM treatment at both the 1 week and terminal time points. This corroborates previous findings in which the LV MM hydrogel was shown to support vascular infiltration[10] and increase vascular density in MI models.[10,14]

Pressure overload on the right ventricle often results in hypertrophy and interstitial fibrosis,[1,3,30,38,61] which affects the right ventricle's ability to pump blood efficiently.[38] MM hydrogels have been shown to effectively diminish hypertrophy and fibrosis in the ischemic myocardium by regulating gene expression related to progressive hypertrophy and decreasing scar formation in the injured tissue.[14] By evaluating the average cardiomyocyte cross-sectional area, we determined that our materials protected against sustained increased afterload as evidenced by a significant decrease in the cross-sectional area compared with the control group. This was further corroborated by our earlier finding of reduced RV free wall thickness, indicating a mitigation of maladaptive hypertrophy. RV fibrotic area can be attributed to the wall stress on the right ventricle, especially near the insertion points where the right ventricle connects with the septum.[62] Although fibrosis typically forms near the insertion points,[62] we found a reduction in fibrosis overall despite location of injection.

We also found that animals treated with the LV MM hydrogel overexpressed cyclin dependent kinase 1 (Cdk1), which has been shown to regulate fibroblast activation, thus reducing fibrosis,[63] and Ccn5, which reverses established fibrosis.[64] The RV MM hydrogel, on the other hand, overexpressed several genes that were responsible for promoting fibrosis (Lox, Postn, and Mmp12).[65-67] However, Postn has also been shown to induce phenotypic changes in RV fibroblasts that are not consistent with typical myofibroblasts.[68,69] RV fibroblasts have been shown to behave similarly to cardiac fibroblasts during the inflammatory phase of MI[69] and have decreased expression of α-SMA and collagen I expression.[68] When Masson's trichrome was used in the current study to identify the interstitial fibrosis in the PAB animals, those injected with either of the MM hydrogels had significantly reduced fibrosis throughout the RV free wall compared with the saline-treated animals. Using immunohistochemistry, we further showed that these materials, compared with saline, aid in the reduction of myofibroblasts as evidenced by a decreased presence of α-SMA at the terminal time point; these are known to synthesize large amounts of collagen and secrete matricellular proteins[38] within the injured right ventricle.

Both MM hydrogels up-regulated genes related to cardiac development compared with saline, specifically Igf2, which is essential for cardiac development and regeneration.[70] This overexpression of Igf2 has been shown to promote cardiomyocyte proliferation in embryonic heart development.[42] Irx1 and Irx2 are a part of the IRX family of genes that are responsible for the development of the cardiac conduction system.[71] Although the down-regulation of these genes may imply the potential for the development of arrythmia, we have shown previously that the injection of a highly spread hydrogel in the myocardium does not alter action potential propagation soon after injection, thus reducing concern for arrythmia due to injection.[13] It has also been shown that the hypermethylation of Irx1 inhibits Cxcl14, which leads to heart failure[72] and the depletion of Irx2 attenuates hypertrophy and improves cardiac systolic function,[73] suggesting that these may be pathways of repair elicited by our materials.

Cardiac contraction plays a vital role in the efficiency of the right ventricle to supply the patient with oxygen-saturated blood in the single-ventricle condition and return desaturated blood to the lungs during pulmonary arterial hypertension. In the

pressure overloaded right ventricle, contractility is severely impaired.[28] In both subacute and chronic models of MI, the MM hydrogel was shown to enhance gene expression related to cardiac contractility.[14,15] We found that the LV MM hydrogel up-regulated the gene Prc1, which is known to stabilize cardiac contraction by regulating sarcomere assembly and conduction system construction,[74] and the gene Cacnag1, which is responsible for creating calcium channels.[75] RV MM-treated animals were shown to up-regulate the gene Piezo2, which has been shown to modulate intracellular calcium handling, which in turn buffers the heart from mechanical stress.[76]

In an earlier in vitro study, we reported that the proteomic makeup of the LV MM and RV MM hydrogels differed, along with some variations in angiogenesis assays,[19] suggesting that the RV MM hydrogel may provide different tissue cues for cardiac repair compared with the previously studied LV MM hydrogel. However, in the current study, no significant differences were found between the LV MM and RV MM hydrogels in any of the functional and histologic metrics assessed.

Overall, due to the less pronounced functional benefit (eg, RVEF, LVEDI) and degree of fibrotic and inflammatory gene expression seen in the RV MM group, these results suggest the LV MM hydrogel provides the greater therapeutic benefit for treating the pressure overloaded right ventricle.

STUDY LIMITATIONS. This study is limited by its use of a small animal PAB model to mimic RVHF after chronic pressure overload. Although we can induce increased afterload in the right ventricle, this model does not fully capture the additional comorbidities such as the volume overload and systemic right ventricle in the pediatric case or the endothelial dysfunction of the lungs in the adult condition. Although we previously saw improvements in negative LV remodeling with the LV MM in female rats, the current study used male rats only. Healing in juvenile rats is also accelerated due to the regenerative capacity of small mammals compared with larger mammals.

CONCLUSIONS

This study is the first, to our knowledge, to assess the efficacy and mechanism of action of an injectable biomaterial in a small animal model of RVHF. We have shown that MM hydrogels improve cardiac function, as evidenced by both echocardiography and MRI, and effectively mitigate negative RV remodeling, which has been shown to affect patients with chronic pressure overload on the right ventricle. These materials are not limited by isolation and expansion requirements of autologous cardiac progenitor cells and therefore could enable the potential to deliver the therapeutic during even earlier stages of pressure overload. Overall, this study provides proof-of-concept for using a pro-reparative, injectable biomaterial for treating RVHF with further potential applications in both pediatric and adult RVHF such as in the cases of tetralogy of Fallot and pulmonary arterial hypertension.

ACKNOWLEDGMENTS The authors thank Josh Mesfin for feedback on the manuscript, the Molecular Imaging Center at Sanford for performing MRI, and Dr Trevor Biddle and the UC San Diego Stem Cell Genomics Core at the Sanford Consortium for Regenerative Medicine for providing RNA-sequencing.

FUNDING SUPPORT AND AUTHOR DISCLOSURES

This research was funded in part by the NIH National Heart, Lung, and Blood Institute (NHLBI) grant R01HL146147 (Drs Davis and Christman). Dr Hunter was supported by an NIH NHLBI Training Grant (T32HL105373) and an NIH NHLBI Predoctoral Fellowship (1F31HL158212). Dr Christman is co-founder, consultant, board member, and holds an equity interest in Ventrix Bio, Inc. All other authors have reported that they have no relationships relevant to the contents of this paper to disclose.

ADDRESS FOR CORRESPONDENCE: Dr Karen L. Christman, Sanford Consortium for Regenerative Medicine, 2880 Torrey Pines Scenic Drive, La Jolla, California 92037, USA. E-mail: kchristman@ucsd.edu. @ChristmanLab.

PERSPECTIVES

COMPETENCY IN MEDICAL KNOWLEDGE: Increased afterload causes negative remodeling in the right ventricle and ultimately failure. Injectable biomaterial therapies to treat RVHF have been highly understudied even though a multitude have been tested to treat left-sided heart failure. This study shows that a pro-reparative injectable biomaterial has the potential to treat RVHF.

TRANSLATIONAL OUTLOOK: The results of this study combined with the demonstration of initial safety and feasibility of the LV-derived MM hydrogel in a phase 1 clinical trial in MI patients suggests the material should be explored in clinical trials for RVHF.

REFERENCES

1. Ryan JJ, Archer SL. The right ventricle in pulmonary arterial hypertension: disorders of metabolism, angiogenesis and adrenergic signaling in right ventricular failure. *Circ Res*. 2014;115:176–188.

2. Garcia AM, Beatty J-T, Nakano SJ. Heart failure in single right ventricle congenital heart disease: physiological and molecular considerations. *Am J Physiol Heart Circ Physiol*. 2020;318:H947–H965.

3. Voelkel NF. How does the pressure-overloaded right ventricle adapt and why does it fail? Macro- and micro-molecular perspectives. In: Friedberg MK, Redington AN, eds. *Right Ventricular Physiology, Adaptation and Failure in Congenital and Acquired Heart Disease*. Springer Science + Business Media; 2018:19–27.

4. Reddy S, Bernstein D. Molecular mechanisms of right ventricular failure. *Circulation*. 2015;132:1734–1742.

5. Dayer N, Ltaief Z, Liaudet L, Lechartier B, Aubert J-D, Yerly P. Pressure overload and right ventricular failure: from pathophysiology to treatment. *J Clin Med*. 2023;12:4722.

6. Simon MA. Assessment and treatment of right ventricular failure. *Nature Rev Cardiol*. 2013;10:204–218.

7. Si MS, Ohye RG. Stem cell therapy for the systemic right ventricle. *Expert Rev Cardiovasc Ther*. 2017;15:813–823.

8. Agarwal U, Smith AW, French KM, et al. Age-dependent effect of pediatric cardiac progenitor cells after juvenile heart failure. *Stem Cells Transl Med*. 2016;5:883–892.

9. Trac D, Maxwell JT, Brown ME, Xu C, Davis ME. Aggregation of child cardiac progenitor cells into spheres activates notch signaling and improves treatment of right ventricular heart failure. *Circ Res*. 2019;124:526–538.

10. Singelyn JM, DeQuach JA, Seif-Naraghi SB, Littlefield RB, Schup-Magoffin PJ, Christman KL. Naturally derived myocardial matrix as an injectable scaffold for cardiac tissue engineering. *Biomaterials*. 2009;30:5409–5416.

11. Singelyn JM, Sundaramurthy P, Johnson TD, et al. Catheter-deliverable hydrogel derived from decellularized ventricular extracellular matrix increases endogenous cardiomyocytes and preserves cardiac function post-myocardial infarction. *J Am Coll Cardiol*. 2012;59:751–763.

12. Seif-Naraghi SB, Singelyn JM, Salvatore MA, et al. Safety and efficacy of an injectable extracellular matrix hydrogel for treating myocardial infarction. *Sci Transl Med*. 2013;5:173ra25.

13. Suarez SL, Rane AA, Muñoz A, et al. Intramyocardial injection of hydrogel with high interstitial spread does not impact action potential propagation. *Acta Biomaterialia*. 2015;26:13–22.

14. Wassenaar JW, Gaetani R, Garcia JJ, et al. Evidence for mechanisms underlying the functional benefits of a myocardial matrix hydrogel for post-MI treatment. *J Am Coll Cardiol*. 2016;67:1074–1086.

15. Diaz MD, Tran E, Spang M, et al. Injectable myocardial matrix hydrogel mitigates negative left ventricular remodeling in a chronic myocardial infarction model. *J Am Coll Cardiol Basic Trans Science*. 2021;6:350–361.

16. Wang RM, Johnson TD, He J, et al. Humanized mouse model for assessing the human immune response to xenogeneic and allogeneic decellularized biomaterials. *Biomaterials*. 2017;129:98–110.

17. Traverse JH, Henry TD, Dib N, et al. First-in-man study of a cardiac extracellular matrix hydrogel in early and late myocardial infarction patients. *J Am Coll Cardiol Basic Trans Science*. 2019;4:659–669.

18. Black BL. Transcriptional pathways in second heart field development. *Semin Cell Dev Biol*. 2007;18:67–76.

19. Hunter JD, Hancko A, Shakya P, et al. Characterization of decellularized left and right ventricular myocardial matrix hydrogels and their effects on cardiac progenitor cells. *J Mol Cell Cardiol*. 2022;171:45–55.

20. Diaz MD, Christman KL. Injectable hydrogels to treat myocardial infarction. In: Serpooshan V, Wu SM, eds. *Cardiovascular Regenerative Medicine: Tissue Engineering and Clinical Applications*. Springer International Publishing; 2019:185–206.

21. He S, Zhang Z, Luo R, Jiang Q, Yang L, Wang Y. Advances in injectable hydrogel strategies for heart failure treatment. *Adv Healthc Mater*. 2023;12:e2300029.

22. Bejleri D, Robeson MJ, Brown ME, et al. In vivo evaluation of bioprinted cardiac patches composed of cardiac-specific extracellular matrix and progenitor cells in a model of pediatric heart failure. *Biomater Sci*. 2022;10:444–456.

23. Maxwell JT, Trac D, Shen M, et al. Electrical stimulation of pediatric cardiac-derived c-kit+ progenitor cells improves retention and cardiac function in right ventricular heart failure. *Stem Cells*. 2019;37:1528–1541.

24. Moroseos T, Mitsumori L, Kerwin WS, et al. Comparison of Simpson's method and three-dimensional reconstruction for measurement of right ventricular volume in patients with complete or corrected transposition of the great arteries. *Am J Cardiol*. 2010;105:1603–1609.

25. Teng WH, McCall PJ, Shelley BG. The utility of eccentricity index as a measure of the right ventricular function in a lung resection cohort. *J Cardiovasc Echogr*. 2019;29:103–110.

26. Krupickova S, Risch J, Gati S, et al. Cardiovascular magnetic resonance normal values in children for biventricular wall thickness and mass. *J Cardiovasc Magn Reson*. 2021;23:1–23.

27. Simon MA, Pinsky MR. Right ventricular dysfunction and failure in chronic pressure overload. *Cardiol Res Pract*. 2011;2011:568095.

28. Arrigo M, Huber LC, Winnik S, et al. Right ventricular failure: pathophysiology, diagnosis and treatment. *Card Fail Rev*. 2019;5:140–146.

29. Hill MR, Simon MA, Valdez-Jasso D, Zhang W, Champion HC, Sacks MS. Structural and mechanical adaptations of right ventricle free wall myocardium to pressure overload. *Ann Biomed Eng*. 2014;42:2451–2465.

30. Files MD, Arya B. Pathophysiology, adaptation, and imaging of the right ventricle in Fontan circulation. *Am J Physiol Heart Circ Physiol*. 2018;315:H1779–H1788.

31. Takele Assefa A, Vandesompele J, Thas O. On the utility of RNA sample pooling to optimize cost and statistical power in RNA sequencing experiments. *BMC Genomics*. 2020;21:1–14.

32. Ko B, Van Raamsdonk JM. RNA sequencing of pooled samples effectively identifies differentially expressed genes. *Biology*. 2023;12:812.

33. Badylak SF, Valentin JE, Ravindra AK, McCabe GP, Stewart-Akers AM. Macrophage phenotype as a determinant of biologic scaffold remodeling. *Tissue Eng Part A*. 2008;14:1835–1842.

34. Sadtler K, Estrellas K, Allen BW, et al. Developing a pro-regenerative biomaterial scaffold microenvironment requires T helper 2 cells. *Science*. 2016;352:366–370.

35. Gu S, Mickael C, Kumar R, et al. The role of macrophages in right ventricular remodeling in experimental pulmonary hypertension. *Pulm Circ*. 2022;12:e12105.

36. Guihaire J, Deuse T, Wang D, et al. Pulmonary hypertension: macrophage infiltration corelates with right ventricular remodeling in an experimental model of pulmonary hypertension. *J Heart Lung Transplant*. 2017;36:S370–S371.

37. Samak M, Fatullayev J, Sabashnikov A, et al. Cardiac hypertrophy: an introduction to molecular and cellular basis. *Med Sci Monit Basic Res*. 2016;22:75.

38. Frangogiannis NG. Fibroblasts and the extracellular matrix in right ventricular disease. *Cardiovasc Res*. 2017;113:1453–1464.

39. Saldin LT, Cramer MC, Velankar SS, White LJ, Badylak SF. Extracellular matrix hydrogels from decellularized tissues: structure and function. *Acta Biomater*. 2017;49:1–15.

40. Meng FW, Slivka PF, Dearth CL, Badylak SF. Solubilized extracellular matrix from brain and urinary bladder elicits distinct functional and phenotypic responses in macrophages. *Biomaterials*. 2015;46:131–140.

41. Wei K-H, Lin I-T, Chowdhury K, et al. Comparative single-cell profiling reveals distinct cardiac resident macrophages essential for zebrafish heart regeneration. *eLife*. 2023;12:e84679.

42. Li P, Cavallero S, Gu Y, et al. IGF signaling directs ventricular cardiomyocyte proliferation during embryonic heart development. *Development*. 2011;138:1795–1805.

43. Liso A, Venuto S, Coda ARD, Giallongo C, Palumbo GA, Tibullo D. IGFBP-6: at the crossroads

of immunity, tissue repair and fibrosis. *Int J Mol Sci*. 2022;23.

44. van Zuylen WJ, Garceau V, Idris A, et al. Macrophage activation and differentiation signals regulate schlafen-4 gene expression: evidence for Schlafen-4 as a modulator of myelopoiesis. *PLoS One*. 2011;6:e15723.

45. Zhang H, Yang K, Chen F, et al. Role of the CCL2-CCR2 axis in cardiovascular disease: pathogenesis and clinical implications. *Front Immunol*. 2022;13:975367.

46. Chang T-T, Chen C, Chen J-W. CCL7 as a novel inflammatory mediator in cardiovascular disease, diabetes mellitus, and kidney disease. *Cardiovasc Diabetol*. 2022;21:185.

47. Heinrichs M, Ashour D, Siegel J, et al. The healing myocardium mobilizes a distinct B-cell subset through a CXCL13-CXCR5-dependent mechanism. *Cardiovasc Res*. 2021;117:2664–2676.

48. Chistiakov DA, Killingsworth MC, Myasoedova VA, Orekhov AN, Bobryshev YV. CD68/macrosialin: not just a histochemical marker. *Lab Invest*. 2017;97:4–13.

49. De Leon-Oliva D, Garcia-Montero C, Fraile-Martinez O, et al. AIF1: function and connection with inflammatory diseases. *Biology (Basel)*. 2023;12.

50. Ebong SJ, Goyert SM, Nemzek JA, Kim J, Bolgos GL, Remick DG. Critical role of CD14 for production of proinflammatory cytokines and cytokine inhibitors during sepsis with failure to alter morbidity or mortality. *Infect Immun*. 2001;69:2099–2106.

51. Puré E, Cuff CA. A crucial role for CD44 in inflammation. *Trends Mol Med*. 2001;7:213–221.

52. Bo Z, Huang S, Li L, et al. EGR2 is a hub-gene in myocardial infarction and aggravates inflammation and apoptosis in hypoxia-induced cardiomyocytes. *BMC Cardiovasc Disord*. 2022;22:373.

53. Lau SL, Yuen ML, Kou CY, Au KW, Zhou J, Tsui SK. Interferons induce the expression of IFITM1 and IFITM3 and suppress the proliferation of rat neonatal cardiomyocytes. *J Cell Biochem*. 2012;113:841–847.

54. Feng Y, Chao W. Toll-like receptors and myocardial inflammation. *Int J Inflam*. 2011;2011:170352.

55. Pal A, Vernon BL, Nikkhah M. Therapeutic neovascularization promoted by injectable hydrogels. *Bioact Mater*. 2018;3:389–400.

56. Christman KL, Vardanian AJ, Fang Q, Sievers RE, Fok HH, Lee RJ. Injectable fibrin scaffold improves cell transplant survival, reduces infarct expansion, and induces neovasculature formation in ischemic myocardium. *J Am Coll Cardiol*. 2004;44:654–660.

57. Chrifi I, Hermkens D, Brandt MM, et al. Cgnl1, an endothelial junction complex protein, regulates GTPase mediated angiogenesis. *Cardiovasc Res*. 2017;113:1776–1788.

58. Yap C, Mieremet A, de Vries CJ, Micha D, de Waard V. Six shades of vascular smooth muscle cells illuminated by KLF4 (Krüppel-Like Factor 4). *Arterioscler Thromb Vasc Biol*. 2021;41:2693–2707.

59. Zhang Q, Chen L, Huang L, et al. CD44 promotes angiogenesis in myocardial infarction through regulating plasma exosome uptake and further enhancing FGFR2 signaling transduction. *Mol Med*. 2022;28:145.

60. Nakao S, Kuwano T, Ishibashi T, Kuwano M, Ono M. Synergistic effect of TNF-α in soluble VCAM-1-induced angiogenesis through α4 integrins1. *J Immunol*. 2003;170:5704–5711.

61. Sutendra G, Dromparis P, Paulin R, et al. A metabolic remodeling in right ventricular hypertrophy is associated with decreased angiogenesis and a transition from a compensated to a decompensated state in pulmonary hypertension. *J Mol Med*. 2013;91:1315–1327.

62. Mikami Y, Cornhill A, Dykstra S, et al. Right ventricular insertion site fibrosis in a dilated cardiomyopathy referral population: phenotypic associations and value for the prediction of heart failure admission or death. *J Cardiovasc Magn Reson*. 2021;23:1–13.

63. Yamamoto T, Matsushima S, Okabe K, et al. Cyclin dependent kinase 1 (CDK1) positively regulates cardiac hypertrophy and fibrosis via TGF-beta pathway. *Eur Heart J*. 2020;41.

64. Jeong D, Lee MA, Li Y, et al. Matricellular protein CCN5 reverses established cardiac fibrosis. *J Am Coll Cardiol*. 2016;67:1556–1568.

65. Nguyen XX, Nishimoto T, Takihara T, Mlakar L, Bradshaw AD, Feghali-Bostwick C. Lysyl oxidase directly contributes to extracellular matrix production and fibrosis in systemic sclerosis. *Am J Physiol Lung Cell Mol Physiol*. 2021;320:L29–L40.

66. Dixon IMC, Landry NM, Rattan SG. Periostin reexpression in heart disease contributes to cardiac interstitial remodeling by supporting the cardiac myofibroblast phenotype. *Adv Exp Med Biol*. 2019;1132:35–41.

67. DeLeon-Pennell KY, Meschiari CA, Jung M, Lindsey ML. Matrix metalloproteinases in myocardial infarction and heart failure. *Prog Mol Biol Transl Sci*. 2017;147:75–100.

68. Imoto K, Okada M, Yamawaki H. Periostin mediates right ventricular failure through induction of inducible nitric oxide synthase expression in right ventricular fibroblasts from monocrotaline-induced pulmonary arterial hypertensive rats. *Int J Mol Sci*. 2018;20.

69. Imoto K, Okada M, Yamawaki H. Characterization of fibroblasts from hypertrophied right ventricle of pulmonary hypertensive rats. *Pflügers Archiv*. 2018;470:1405–1417.

70. Díaz Del Moral S, Benaouicha M, Muñoz-Chápuli R, Carmona R. The insulin-like growth factor signalling pathway in cardiac development and regeneration. *Int J Mol Sci*. 2021;23.

71. Hu W, Xin Y, Zhang L, Hu J, Sun Y, Zhao Y. Iroquois Homeodomain transcription factors in ventricular conduction system and arrhythmia. *Int J Med Sci*. 2018;15:808–815.

72. Zeng L, Gu N, Chen J, Jin G, Zheng Y. IRX1 hypermethylation promotes heart failure by inhibiting CXCL14 expression. *Cell Cycle*. 2019;18:3251–3262.

73. Ma Z-G, Yuan Y-P, Fan D, et al. IRX2 regulates angiotensin II-induced cardiac fibrosis by transcriptionally activating EGR1 in male mice. *Nature Communications*. 2023;14:4967.

74. Peng X, Feng G, Zhang Y, Sun Y. PRC1 stabilizes cardiac contraction by regulating cardiac sarcomere assembly and cardiac conduction system construction. *Int J Mol Sci*. 2021;22.

75. Berecki G, Helbig KL, Ware TL, et al. Novel missense CACNA1G mutations associated with infantile-onset developmental and epileptic encephalopathy. *Int J Mol Sci*. 2020;21.

76. Zechini L, Camilleri-Brennan J, Walsh J, et al. Piezo buffers mechanical stress via modulation of intracellular Ca2+ handling in the Drosophila heart. *Front Physiol*. 2022;13:1003999.

KEY WORDS biomaterial, extracellular matrix, hydrogel, negative right ventricular remodeling, right ventricle

APPENDIX For supplemental tables, please see the online version of this paper.